Laboratory Investigation (2017) 97, 84–92

Automated evaluation of liver fibrosis in thioacetamide, carbon tetrachloride, and bile duct ligation rodent models using second-harmonic generation/two-photon excited fluorescence microscopy

Feng Liu[1], Long Chen[1], Hui-Ying Rao[1], Xiao Teng[2], Ya-Yun Ren[2], Yan-Qiang Lu[2], Wei Zhang[1], Nan Wu[1], Fang-Fang Liu[3] and Lai Wei[1]

Animal models provide a useful platform for developing and testing new drugs to treat liver fibrosis. Accordingly, we developed a novel automated system to evaluate liver fibrosis in rodent models. This system uses second-harmonic generation (SHG)/two-photon excited fluorescence (TPEF) microscopy to assess a total of four mouse and rat models, using chemical treatment with either thioacetamide (TAA) or carbon tetrachloride (CCl_4), and a surgical method, bile duct ligation (BDL). The results obtained by the new technique were compared with that using Ishak fibrosis scores and two currently used quantitative methods for determining liver fibrosis: the collagen proportionate area (CPA) and measurement of hydroxyproline (HYP) content. We show that 11 shared morphological parameters faithfully recapitulate Ishak fibrosis scores in the models, with high area under the receiver operating characteristic (ROC) curve (AUC) performance. The AUC values of 11 shared parameters were greater than that of the CPA (TAA: 0.758–0.922 *vs* 0.752–0.908; BDL: 0.874–0.989 *vs* 0.678–0.966) in the TAA mice and BDL rat models and similar to that of the CPA in the TAA rat and CCl_4 mouse models. Similarly, based on the trends in these parameters at different time points, 9, 10, 7, and 2 model-specific parameters were selected for the TAA rats, TAA mice, CCl_4 mice, and BDL rats, respectively. These parameters identified differences among the time points in the four models, with high AUC accuracy, and the corresponding AUC values of these parameters were greater compared with those of the CPA in the TAA rat and mouse models (rats: 0.769–0.894 *vs* 0.64–0.799; mice: 0.87–0.93 *vs* 0.739–0.836) and similar to those of the CPA in the CCl_4 mouse and BDL rat models. Similarly, the AUC values of 11 shared parameters and model-specific parameters were greater than those of HYP in the TAA rats, TAA mice, and CCl_4 mouse models and were similar to those of HYP in the BDL rat models. The automated evaluation system, combined with 11 shared parameters and model-specific parameters, could specifically, accurately, and quantitatively stage liver fibrosis in animal models.

Laboratory Investigation (2017) **97,** 84–92; doi:10.1038/labinvest.2016.128; published online 5 December 2016

Liver fibrosis is the eventual outcome of many chronic liver diseases, regardless of the etiology of injury. Fibrosis results from an imbalance in the normal wound-healing response, generating an abnormal continuation of fibrogenesis, that is, connective tissue production and deposition. Liver fibrosis and its end-stage outcomes, cirrhosis or hepatocellular carcinoma, represent a serious global health-care burden.[1,2] While anti-viral treatments are able to inhibit fibrosis in both chronic hepatitis B (CHB) and chronic hepatitis C (CHC) patients, the disease does not regress. There are also no effective treatments for liver fibrosis that is not caused by infectious agents, such as non-alcoholic steatohepatitis.[3] Therefore, pharmacological therapies that prevent the progression toward cirrhosis or induce regression of advanced fibrosis and cirrhosis are urgently needed.[4,5]

Because many factors complicate studies of liver fibrosis in human subjects, rodent models of liver fibrosis that mimic human liver diseases have been developed and used for several decades to study fibrogenesis. These models provide a useful platform for developing novel antifibrotic therapeutic

[1]Peking University People's Hospital, Peking University Hepatology Institute, Beijing Key Laboratory of Hepatitis C and Immunotherapy for Liver Diseases, Beijing, China; [2]Hangzhou Choutu Technology, Hangzhou, China and [3]Department of Pathology, Peking University People's Hospital, Beijing, China
Correspondence: Professor L Wei, Peking University People's Hospital, Peking University Hepatology Institute, Beijing Key Laboratory of Hepatitis C and Immunotherapy for Liver Diseases, No.11, Xizhimen South Street, Beijing 100044, China.
E-mail: weilai@pkuph.edu.cn

Received 16 June 2016; revised 16 October 2016; accepted 1 November 2016

approaches and testing new drugs.[6,7] However, an appropriate staging system (such as Ishak) or other quantitative methods for examining liver fibrosis (measurement of the collagen proportional area (CPA) or hydroxyproline (HYP) content) have not been extensively studies in animal models. Therefore, the precise, accurate, and dynamic evaluation of the degree of liver fibrosis in animal models would be very valuable for the development of more effective drugs.

Second-harmonic generation (SHG) is a very sensitive method used to detect dissymmetry in structures and is suitable for imaging collagen fibers with non-centrosymmetric structures. Organizational structures and autofluorescence properties are observed using two-photon excited fluorescence (TPEF) imaging when the sample is irradiated with an exogenous or endogenous laser.

SHG/TPEF has been successfully used to assess fibrosis in various tissues and organs, including the liver. Compared with traditional staining, such as Masson's trichrome and Sirius red staining, SHG/TPEF is a sensitive, quantitative, and automated tool that characterizes collagen in fibrotic tissues.[8–11] A series of automated assessment methods combining the quantification of histopathological architectural parameters imaged using SHG/TPEF was reported as useful in core biopsy evaluations of fibrosis in CHB and CHC patients.[12–15] However, it is not clear whether this purely quantitative method can be used to evaluate liver fibrosis models.

When evaluating the process of fibrogenesis, the results should be replicable in a minimum of two models using different fibrosis-inducing stimuli. Therefore, the main aim of this study was to develop an automated evaluation system for liver fibrosis by combining SHG microscopy and the adaptive quantification algorithm to identify collagen progression patterns that are shared by or specific to three different fibrotic animal models. With the aim of increasing the diagnostic precision compared with the available liver fibrosis staging methods, the results were compared with the CPA method.

MATERIALS AND METHODS

Ethics Statement

The care and use of animals completely complied with the relevant governmental and institutional policies. All animals were supplied by Beijing Vital River Laboratory Animal Technology, China. The animals were housed at 25 °C with a 12 h light–dark cycle and provided standard chow and water *ad libitum* until the time of the study. All study protocols were approved by the Animal Experimental Ethical Committee of Peking University People's Hospital (No. 2014-23).

Animal Models of Liver Fibrosis

TAA Rat and Mouse Models

Male Wistar rats weighing 200–250 g were intoxicated with thioacetamide (TAA) (Sigma, St Louis, MO, USA) for 18 weeks. Initially, 0.03% TAA was administered to all groups via the drinking water. Thereafter, the TAA concentrations were adapted weekly according to the body weight, aiming to maintain individual body weights between the preset limits of 200 and 250 g, as described previously.[16] Practically, the TAA concentrations were increased or decreased by 50% if the weight increased or decreased more than 20 g weekly or if the overall weight increased or decreased more than 60 g. The rats were killed at 2, 4, 6, 8, 12, 16, and 18 weeks ($n=12$ per week) using sodium pentobarbital. Ten control rats were also used at week 0 after the experiment was initiated.

Six-eight-week-old male C57Bl/6 mice were exposed to TAA (Sigma) dissolved in drinking water (300 mg/l) for 18 weeks to induce hepatic fibrosis, whereas the controls received an equal volume of water. The mice were killed at 2, 4, 6, 8, 12, 16, and 18 weeks ($n=8$ per week) using sodium pentobarbital. Six control mice were also used at week 0 after the experiment was initiated.

CCl_4 Mouse Model

Six-week-old male BALB/c mice were intraperitoneally injected with carbon tetrachloride (CCl_4) (1 ml/kg BW dissolved in olive oil; final concentration of 10%) twice per week for 16 weeks to induce liver fibrosis. The mice were killed at 1, 2, 4, 6, 8, 12, and 16 weeks ($n=8$ per week) using sodium pentobarbital. Six control mice were also used at week 0 after the experiment was initiated.

BDL Rat Model

Bile duct ligation (BDL)-induced fibrosis was initiated as described previously.[17] Liver fibrosis was induced in age-matched male Sprague–Dawley rats (250–300 g) using BDL under isoflurane anesthesia. This procedure generates a successful ligation. The bile duct was similarly manipulated but not ligated in the SHAM rats. The rats were killed at 1, 2, 3, 4, and 5 weeks ($n=12$ per week) using sodium pentobarbital. Ten control rats were also killed at week 0.

All animals were anesthetized and blood was collected at the time of killing to measure the serum alanine aminotransferase (ALT) and γ-glutamyl transpeptidase (GGT) levels. Liver specimens from the left lateral lobe of each animal were formalin-fixed, paraffin-embedded, and sectioned for direct SHG imaging, hematoxylin and eosin, Masson's trichrome, or picrosirius red staining (PS) for histological analysis. Inflammatory activities and fibrosis were semiquantitatively evaluated by pathologists using the Ishak scoring system.[18] The remaining portion of the liver was frozen in liquid nitrogen and stored at − 80 °C until the HYP content was determined.

In the toxin treatment models, including the TAA Wistar rats, TAA mice, and CCl_4 mouse models, samples were collected for further analysis at five time points, including the untreated animals at week 0 and the treated animals at weeks 4, 8, 12 and 16, and samples were collected from the BDL rat

model at six time points, including the untreated animals at week 0 and the treated animals at weeks 1, 2, 3, 4, and 5.

Determination of the HYP Content

The extent of the liver fibrosis was also determined by estimating the total liver collagen content, as reflected by measurements of the HYP content in the liver. HYP content was measured using a test kit (Nanjing Jiancheng Bioengineering Institute, Nanjing, China). Briefly, the liver tissue samples were weighed and hydrolyzed with NaOH to release HYP from collagen. Next, HYP was oxidized with chloramine T, followed by a reaction with paradimethylaminobenzaldehyde at 65 °C to develop a mauve color. The absorbance was measured at 550 nm, and the HYP concentration was calculated by comparing the value with standards.[19]

Image Acquisition System

Images of unstained sections of the tissue samples were acquired using a Genesis (HistoIndex, Singapore, Singapore) system. SHG microscopy was used to visualize collagen, and the other cell structures were visualized with TPEF microscopy.

The samples were excited with a 780 nm laser, the SHG signals were recorded at 390 nm, and the TPEF signals were recorded at 550 nm. The images were acquired at $\times 20$ magnification with 512×512 pixel resolution, and each image had a dimension of $200 \times 200\,\mu m^2$.[9,10] Ten five-by-five multitile images ($1 \times 1\,mm^2$ each) were acquired for each human biopsy sample to image most of the sample areas, with a final image size of $10\,mm^2$.

Image Quantification

The total collagen percentages and other previously reported collagen parameters,[12] including specific string and collagen connectivity-related measurements, were used to assess fibrosis progression in the various animal models and were correlated with the corresponding Ishak fibrosis stages.

One hundred collagen morphological parameters were used in this study (Supplementary Table 1). In addition to measuring the CPA as a single parameter, collagen further subcategorized into two different groups, namely, distributed collagen (fine collagen) and aggregated collagen (large patches).[10] In this study, we also implemented liver-specific collagen features including portal collagen (portal expansion), septal collagen (bridging fibrosis), and fibrillar collagen (fine collagen distributed in the pericellular/perisinusoidal space).

Model Construction and Statistical Analysis

The support vector machine (SVM) model method was used to compare the Ishak fibrosis stage and the time point after modeling in each sample with the morphometric collagen features extracted from the images. A hyperplane was constructed to classify optimally the fibrosis stages or modeling time points for the subjects based on the feature values in the m-dimensional space ($m \geq n$). The radial basis function kernel was used as the distance measure between two subject vectors x and x', that is,

$$K(x, x') = \exp\left(-\frac{\|x - x'\|^2}{2\sigma^2}\right)$$

where σ controlled the width of the kernel.[14,20]

The receiver operating characteristic (ROC) curve was used to illustrate the performance of the classifier model, as its discrimination threshold varied. The area under the ROC curve (AUC) was used to illustrate the performance of the classifier model, as its discrimination threshold varied. The advantages of different methods were illustrated by comparing the AUC values among methods using the collagen

Table 1 ALT and GGT levels and HAIs of all experimental groups at different time points after the induction of liver fibrosis[a]

Week[b]	TAA rats			TAA mice			CCl_4 mice			BDL rats		
	ALT	GGT	HAI	ALT	GGT	HAI	ALT	GGT	HAI	ALT	GGT	HAI
0	44.1 ± 11.1	0.4 ± 0.4	0 ± 0	33.3 ± 9.6	0.6 ± 0.5	0 ± 0	32.0 ± 9.8	1.5 ± 1.4	0 ± 0	52.6 ± 8.8	0.4 ± 0.3	0 ± 0
1	48.8 ± 16.0	2.1 ± 1.9	2 ± 2	199.7 ± 105.7[c]	0.8 ± 0.7	7 ± 5	144.6 ± 52.0[c]	0.8 ± 0.5	6 ± 2	140.6 ± 87[c]	47.9 ± 25.4[d]	4 ± 2
2	56.9 ± 13.3	4.7 ± 4.1	8 ± 3	179.9 ± 83.7[c]	0.5 ± 0.5	7 ± 5	118.6 ± 28.3[c]	0.6 ± 0.3	6 ± 6	157.3 ± 55.1[c]	41.8 ± 20.5[d]	6 ± 2
3	56.9 ± 19.4	8.0 ± 5.7	8 ± 3	164.9 ± 62[c]	1.7 ± 1.7	7 ± 4	103.0 ± 39.7[c]	0.4 ± 0.4	9 ± 3	151.8 ± 41.6[c]	60.2 ± 19.7[d]	8 ± 2
4	55.1 ± 16.8	7.4 ± 7.2	9 ± 4	129.2 ± 26.3[c]	0.5 ± 0.4	8 ± 5	180.0 ± 28.1[c]	0.6 ± 0.4	11 ± 1	164.2 ± 55.2[c]	62.4 ± 29.6[d]	8 ± 1
5	NA	NA	NA	NA	NA	NA	NA	NA	NA	153.9 ± 43.6[c]	66.0 ± 35.0[d]	9 ± 2

Abbreviations: ALT, alanine aminotransferase; BDL, bile duct ligation; CCl_4, carbon tetrachloride; GGT, γ-glutamyl transpeptidase; HAI, histological activity index; NA, not applicable; TAA, thioacetamide.
[a]The values are expressed as means plus/minus s.e.
[b]For the TAA rat, TAA mouse, and CCl_4 mouse models, 0, 1, 2, 3, and 4 correspond to weeks 0, 4, 8, 12, and 16, respectively, whereas for the BDL rat model, 0, 1, 2, 3, 4, and 5 correspond to weeks 0, 1, 2, 3, 4, and 5, respectively.
[c]$P < 0.05$ *vs* week 0.
[d]$P < 0.05$ *vs* week 0.

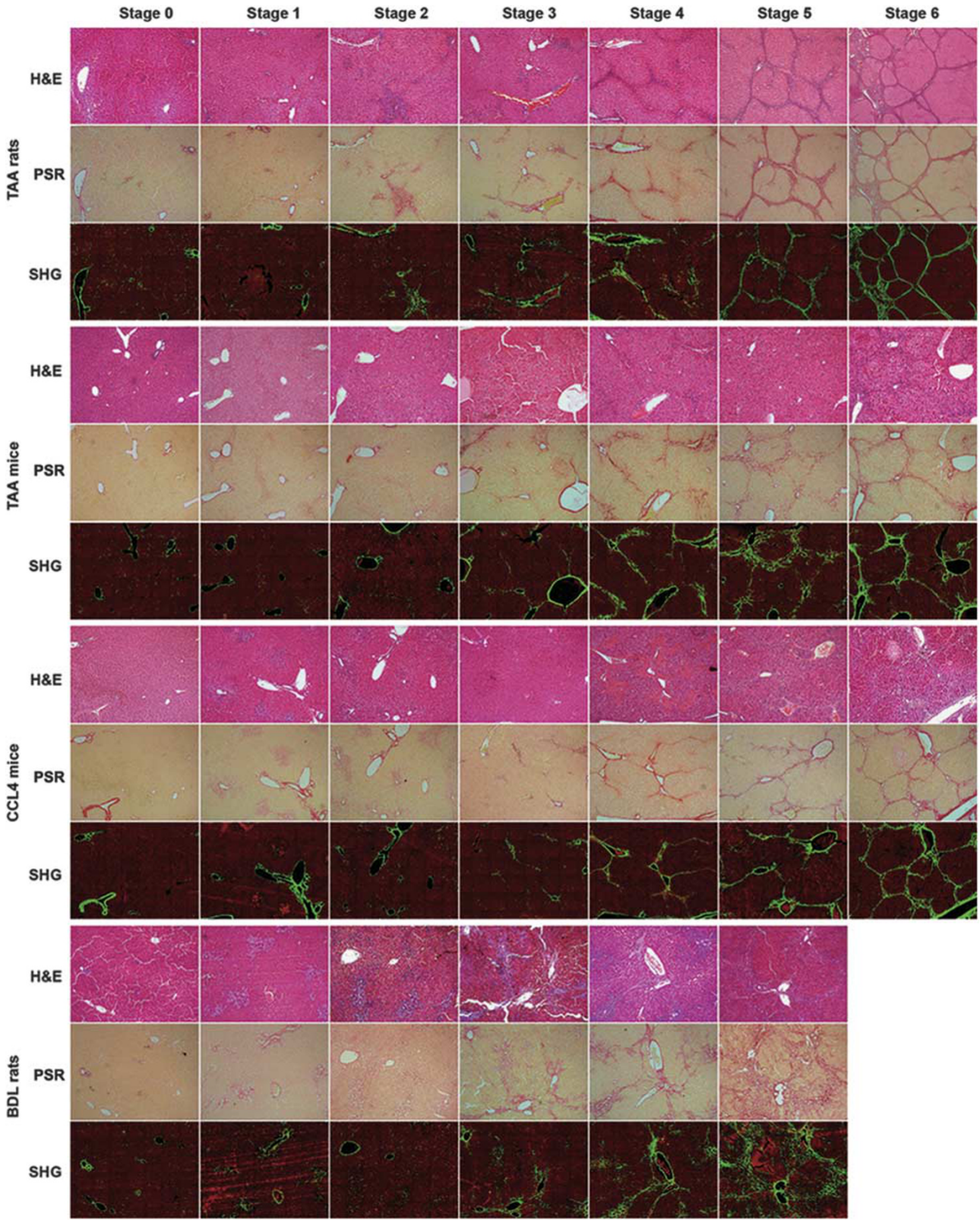

Figure 1 Comparison of histopathological staining (hematoxylin and eosin (H&E) and picrosirius red staining (PS)) and the second-harmonic generation (SHG)/two-photon excited fluorescence (TPEF) microscopy images of tissues at different Ishak stages (×100 magnification). BDL, bile duct ligation; CCl_4, carbon tetrachloride; TAA, thioacetamide.

parameters, CPA and HYP content. After the assumption that the collagen features were normally distributed was accepted by Lilliefors test, and Student's *t*-test was used to estimate the statistical significance of the differences in the collagen string features among the different Ishak fibrosis stages and different time points after modeling. Furthermore, a multiple testing correction was used for the statistical tests. The Spearman's nonparametric correlation coefficients and the significance of the correlations were calculated. The statistical significance level was set to $P<0.05$.

RESULTS

ALT and GGT Levels and the HAI of Liver Injury

The ALT (IU/l) and GGT (IU/l levels and histological activity indices (HAIs) for all experimental groups are shown in Table 1. These values delineate the course of liver injury following the establishment of the models listed above. There were significant increases in the ALT levels in the TAA mice, CCl_4 mice, and BDL rat groups compared with the week 0 control ($P<0.05$), but this increase was not observed in the TAA rat group. A significant increase in the GGT levels was only observed in the BDL rat group compared with the week 0 control ($P<0.05$), but was not observed in the other groups.

Over time, the HAI increased in all experimental groups, but there were no further increases until 12 weeks in the TAA rats and mice, and until 4 weeks in the BDL rats.

SHG/TPEF *vs* Conventional Histological Imaging

As the time after chemical treatment (TAA or CCl_4) and BDL increased, the microscopic features of the liver changed from normal tissue to fibrosis and cirrhosis. The control mice and rats displayed a normal histology and the lobular architecture was preserved. No cellular damage was present.

TAA model

After 6 weeks of TAA intoxication, PS staining primarily showed stage 2 periportal fibrosis. At 12 weeks, PS staining illustrated fine thread-like fibrosis and the formation of portal–portal and portal–central septa that were mainly described as stage 5 fibrosis. At 16 weeks, fully established stage 6 cirrhosis was present in all animals, along with the formation of portal–central shunts (Figure 1).

CCl_4 model

Two weeks after CCl_4 administration, PS staining revealed stage 1 or 2 fibrotic changes in the centrolobular area. Eight weeks after CCl_4 administration, the liver architecture primarily changed to stage 4 and exhibited reversed lobulation, because of the development of centrocentral fibrotic linkages. After 12 weeks, the reversed lobulation was accentuated, along with the development of thin fibrotic centroportal septa in addition to the centrocentral fibrotic linkages. However, after 16 weeks, all mice had homogeneous characteristics reflecting stage 6 cirrhosis (Figure 1).

BDL model

The enlargement of the portal tracts appeared as early as 1 week after BDL. This enlargement was accompanied by dilation of the bile canaliculi and proliferation of the smaller bile ducts. Periportal fibrosis developed 1 to 3 weeks after BDL induction. After 3 weeks, the periportal alterations were accompanied by fibrotic changes described as Ishak stage 3 that evolved into Ishak stage 5 by 5 weeks after BDL (Figure 1).

SHG and TPEF microscopy were used to quantify simultaneously the changes in fibrillar collagen during liver fibrosis progression. We observed that fibrillar collagen is correctly detected by the SHG signals in the liver tissue, based on the images of the histological staining in the different animal fibrosis models (Figure 1).

Eleven Shared Morphological Parameters that Faithfully Recapitulate Ishak Fibrosis Scores

Liver fibrosis progression was quantified using the SHG/TPEF system by examining the collagen levels and morphology. A list of 100 collagen architectural parameters (Supplementary Table 1), categorized into four groups, namely, overall, portal, septal, and fibrillar collagen, were identified through image acquisition and processing and translated into quantitative parameters to understand their relationships with the Ishak stages.

We selected separate parameters for each animal model. Based on their trends with respect to the fibrosis stages and systemic AUC analyses, 36, 18, 35, and 40 parameters were selected for the TAA rats, TAA mice, CCl_4 mice, and BDL rats, respectively (Supplementary Table 2). In the TAA rats and mice, more portal collagen parameters were consistently elevated throughout the experiment (NoStrP for all stages, $P<0.05$) (Figure 2); however, more parameters were focused on the overall, portal, and septal collagen in the CCl_4 mice and BDL rats (StrArea for all stages, $P<0.01$). These differences may be related to the different treatment mechanisms.

Among all of these parameters, we found that 11 were shared by all models, including SHG, StrArea, NoXlink, NoStrP, NoShortStrP, NoLongStrP, NoThickStrP, NoThickStrPA, StrLengthPA, StrWidthPA, and FibrillarAGG (Table 2), mainly for portal collagen. The flow chart is shown in Figure 3. Our experiments show that these 11 parameters faithfully recapitulate the Ishak fibrosis scores.

The Eleven Shared Parameters Exhibit Superior Performance Compared with the CPA and HYP Content in Evaluating Liver Fibrosis

The performance of the shared parameters *vs* CPA for scoring fibrosis were evaluated using an ROC analysis. In the TAA mouse model, the AUC values of the shared parameters for the detection of different stages were >0.8, whereas the AUC of CPA dropped to 0.6 (stage 0 *vs* 1, 2, 3, 4, 5, and 6; stages 0 and 1 *vs* 2, 3, 4, 5, and 6; and stages 0, 1, 2, 3, 4, and 5 *vs* 6). In

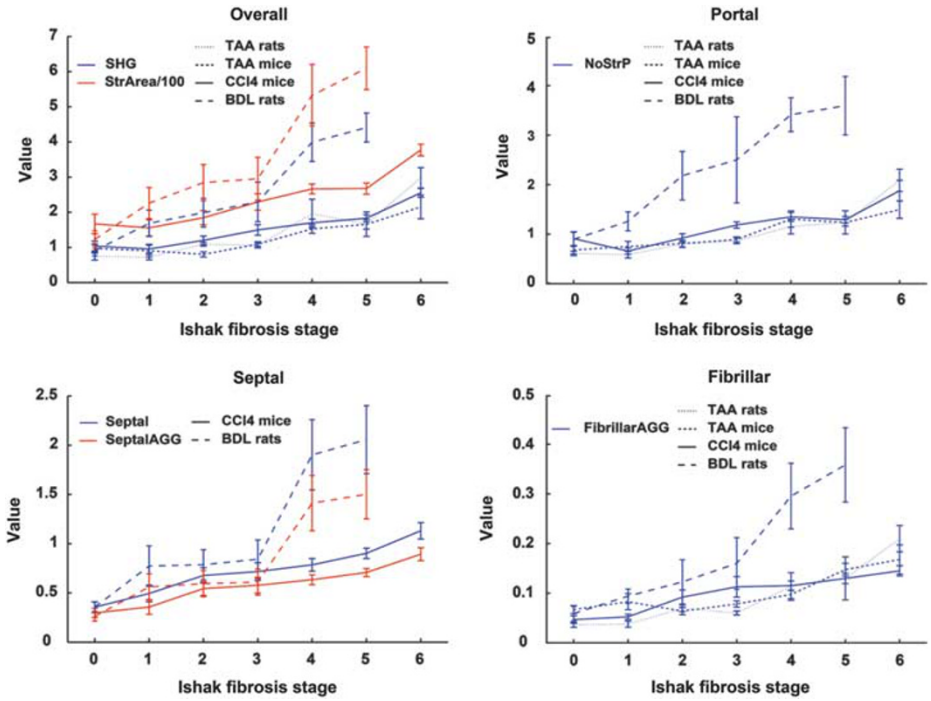

Figure 2 Changes in collagen features along with the Ishak fibrosis stages in different areas of the liver tissues from each animal model. BDL, bile duct ligation; CCl_4, carbon tetrachloride; TAA, thioacetamide.

Table 2 Abbreviations for the 11 shared parameters

No.	Abbreviation	Description
1	SHG	SHG percentage
2	StrArea	String area
3	NoXlink	Number of crosslinks
4	NoStrP	Number of strings (portal)
5	NoShortStrP	Number of short dtrings (portal)
6	NoLongStrP	Number of long strings (portal)
7	NoThickStrP	Number of thick strings (portal)
8	NoThickStrPA	Number of thick strings (portal and aggregated)
9	StrLengthPA	String length (portal and aggregated)
10	StrWidthPA	String width (portal and aggregated)
11	FibrillarAGG	Fibrillar aggregated collagen percentage

Abbreviation: SHG, second-harmonic generation.

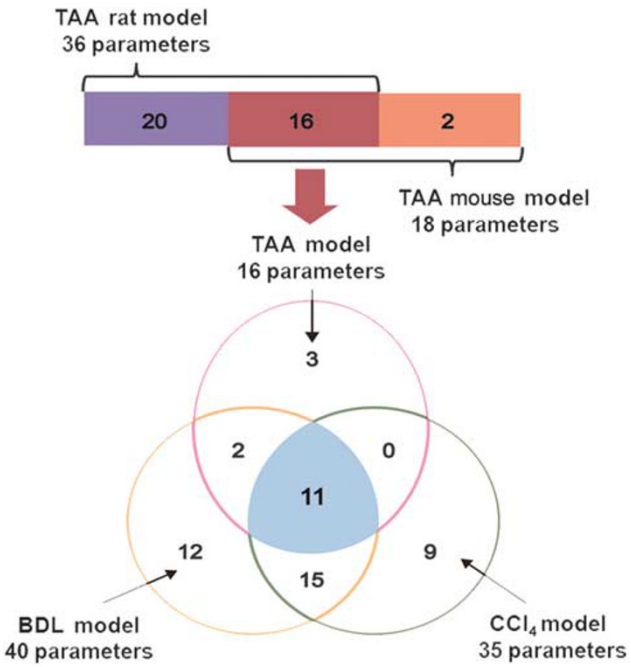

Figure 3 Analysis of the shared fibrosis parameters among the four animal models. Parameters of 36, 18, 35, and 40 were selected for the thioacetamide (TAA) rats, TAA mice, carbon tetrachloride (CCl_4) mice, and bile duct ligation (BDL) rats, respectively. Eleven of these parameters were shared by all models.

the BDL rat model, the AUC values of the shared parameters ranged from 0.99 to 0.87, whereas the AUC values of CPA were reduced (0.97–0.68) and as low as 0.678 (stages 0, 1, 2, 3, 4 *vs* 5). In contrast, the shared parameters achieved similar AUC values to that of CPA (AUC: 0.7–0.9) in the CCl_4 mice and TAA rat models (AUC: 0.7–0.9) (Table 3).

The performances of the 11 shared parameters *vs* the HYP content for fibrosis scoring were also evaluated using an ROC analysis. The AUC values of the shared parameters were greater than HYP in the TAA rats (0.758–0.922 *vs* 0.719–0.869), TAA mice (0.808–0.945 *vs* 0.339–0.893), and CCl_4 mice (0.713–0.954 *vs* 0.159–0.914) models, and similar

Table 3 AUC values of CPA and HYP content and the shared parameters in each Ishak fibrosis stage in the four fibrosis models

Fibrosis stage	TAA rats			TAA mice			CCl_4 mice			BDL rats		
	CPA	HYP	Shared parameters	CPA	HYP	Shared parameters	CPA	HYP	Shared parameters	CPA	HYP	Shared parameters
0 *vs* 1, 2, 3, 4, 5, 6	0.752	0.869	0.758	0.682	0.339	0.853	0.904	0.769	0.904	0.966	0.92	0.989
0, 1 *vs* 2, 3, 4, 5, 6	0.875	0.809	0.892	0.674	0.522	0.833	0.888	0.159	0.954	0.832	0.934	0.936
0, 1, 2 *vs* 3, 4, 5, 6	0.827	0.817	0.895	0.847	0.893	0.942	0.893	0.914	0.899	0.888	0.908	0.901
0, 1, 2, 3 *vs* 4, 5, 6	0.885	0.795	0.922	0.874	0.892	0.945	0.832	0.887	0.784	0.958	0.969	0.972
0, 1, 2, 3, 4 *vs* 5, 6	0.842	0.719	0.89	0.793	0.806	0.876	0.753	0.898	0.713	0.678	0.902	0.874
0, 1, 2, 3, 4, 5 *vs* 6	0.908	0.804	0.916	0.606	0.802	0.808	0.865	0.765	0.863			

Abbreviations: AUC, area under ROC curve; BDL, bile duct ligation; CCl_4, carbon tetrachloride; CPA, collagen proportionate area; HYP, hydroxyproline; TAA, thioacetamide.

Table 4 AUC values of CPA and HYP content and the different collagen parameters at the different time points after the induction of liver fibrosis

Week[a]	TAA rats			TAA mice			CCl_4 mice			BDL rats		
	CPA	HYP	1–9	CPA	HYP	1–10	CPA	HYP	1–7	CPA	HYP	1–2
0 *vs* 1, 2, 3, 4, 5	0.64	0.833	0.856	0.748	0.286	0.93	0.878	0.397	0.949	0.97	0.928	0.987
0, 1 *vs* 2, 3, 4, 5	0.799	0.782	0.88	0.836	0.912	0.912	0.862	0.929	0.879	0.87	0.913	0.822
0, 1, 2 *vs* 3, 4, 5	0.676	0.741	0.769	0.802	0.78	0.909	0.767	0.847	0.751	0.878	0.917	0.725
0, 1, 2, 3 *vs* 4, 5	0.625	0.674	0.894	0.739	0.511	0.87	0.833	0.396	0.983	0.974	0.955	0.803
0, 1, 2, 3, 4 *vs* 5	NA	NA	NA	NA	NA	NA	NA	NA	NA	0.411	0.922	0.793

Abbreviations: AUC, area under ROC curve; BDL, bile duct ligation; CCl_4, carbon tetrachloride; CPA, collagen proportionate area; HYP, hydroxyproline; NA, not applicable; TAA, thioacetamide.
[a]For the TAA rat, TAA mouse, and CCl_4 mouse models, 0, 1, 2, 3, and 4 correspond to weeks 0, 4, 8, 12, and 16, respectively, whereas for the BDL rat model, 0, 1, 2, 3, 4, and 5 correspond to weeks 0, 1, 2, 3, 4, and 5, respectively.

AUC values as HYP were achieved in the BDL rats group (0.902–0.969 *vs* 0.874–0.989) (Table 3). Thus, we revealed that the shared parameters can potentially differentiate the various stages of fibrosis in four different liver fibrosis models.

The Model-Specific Parameters Further Improve the Diagnostic Reliability

In addition to the comparison with the Ishak stages, we also performed a test using different time points after modeling. Based on their trends with respect to time after modeling and systemic AUC analyses, 12, 20, 9, and 18 parameters were selected for the TAA rats, TAA mice, CCl_4 mice, and BDL rat models, respectively. However, no common parameters were shared by the four models with respect to the stage evaluation. We designed a class-specific ensemble feature selection framework to identify the most important parameters of the extracted parameters, and then 9, 10, 7, and 2 parameters were selected for the TAA rats, TAA mice, CCl_4 mice, and BDL rat models, respectively (Supplementary Table 3). Next, using the SVM model, these model-specific parameters were shown to identify differences among all time points in the four different fibrosis models, with high AUC accuracy (AUC: 0.751–0.987, $P<0.05$) (Table 4).

The performances of the model-specific parameters *vs* CPA for fibrosis scoring were evaluated with an ROC analysis. The AUC values of the model-specific parameters for the detection of different time points after modeling were maintained at higher values than those of the CPA in the TAA rats and mouse models, and were similar in the CCl_4 mice and BDL rat models. Furthermore, in the BDL rat model, the AUC values of the model-specific parameters were greater than the values obtained for the CPA (0.793 *vs* 0.411). The performances of the model-specific parameters *vs* the HYP content for fibrosis scoring were also evaluated with an ROC analysis. The AUC values of the model-specific parameters for the detection of different time points after

modeling were maintained at higher values than HYP in the TAA rats (0.769–0.894 *vs* 0.674–0.833), TAA mice (0.87–0.93 *vs* 0.286–0.912), and CCl_4 mice (0.751–0.983 *vs* 0.397–0.929), and AUC values similar to the values obtained for HYP were achieved in the BDL rats group (0.725–0.987 *vs* 0.913–0.955) (Table 4). Thus, we showed that the model-specific parameters can potentially differentiate fibrosis at different time points in four different liver fibrosis models.

DISCUSSION

In this study, we successfully acquired SHG and TPEF images from TAA, CCl_4, and BDL rodent models and established an automated evaluation system that is superior to the Ishak staging scores and CPA evaluation.

We first showed the feasibility of our SHG/TPEF microscopy technique in monitoring liver fibrosis progression in the TAA, CCl_4, and BDL animal models by comparing this system with the conventional Ishak staging/histopathological scoring system. Based on their trends with respect to the fibrosis stages and systemic AUC analyses, 11 shared parameters were selected and faithfully recapitulated the Ishak scores. The TAA, CCl_4, and BDL models have traditionally been used as the most widely used experimental models of fibrosis, and the collagen distribution profiles in liver fibrosis are significantly different among these models.[21] However, periportal fibrosis is a common feature of these models, and the results showed that 7 out of 11 parameters (NoStrP, NoShortStrP, NoLongStrP, NoThickStrP, NoThickStrPA, StrLengthPA, and StrWidthPA) were primarily derived from portal collagen. The collagen distribution characteristics and high AUC values suggest that these parameters have more discriminative power for precisely reflecting the dynamics of fibrosis progression in different models, and we may be able to identify the patterns for different causes of liver fibrosis and produce a standardized system for evaluating different pathologies using specialized algorithms.

Methods for quantifying the CPA and HYP content, which are also quantitative approaches for evaluating the collagen levels in the liver, were developed to obtain more accuracy and objectivity in the quantification of fibrosis.[22] Furthermore, we compared the performance of these 11 shared parameters with the CPA and HYP content. SHG imaging might improve the issues listed above, and the 11 shared parameters exhibited similar performance to CPA in the CCl_4 mice and TAA rat models and superior performance to CPA in the TAA mice and BDL rats. Moreover, the 11 shared parameters exhibited similar performance to the HYP content in the BDL rats and superior performance to the HYP content in the TAA rats, TAA mice, and CCl_4 mice. Collectively, these results suggest that the 11 shared parameters might replace the Ishak score, and the CPA or HYP content for evaluating liver fibrosis in the four different liver fibrosis models.

Histological staging is a fundamental concept included in our automated evaluation system, but the progression of fibrosis at different time points after modeling should also be considered when evaluating liver fibrosis. Therefore, based on their trends with respect to the different time points after modeling and AUC analyses, model-specific parameters were selected and shown to identify the differences among all time points in the four different fibrosis models with high AUC accuracy. These model-specific parameters, which mainly focus on string collagen in the TAA model, portal collagen in the CCl_4 model, and aggregated collagen in the BDL model, may be related to the specific collagen distribution patterns in the different models. Furthermore, the AUC values of the model-specific parameters were maintained at higher values than CPA in the TAA rats and mouse models and were similar to the CPA in the CCl_4 mice and BDL rat models. Similarly, the model-specific parameters achieved similar performance as the HYP content in the BDL rats and superior performance to the HYP content in the TAA rats, TAA mice, and CCl_4 mice. Thus, we showed that the model-specific parameters can potentially differentiate fibrosis at different time points in four different liver fibrosis models.

We combined the shared and model-specific parameters in the automated evaluation system. The system standardizes the measurements, is highly quantitative, and provides a unique method that precisely reflects the fibrosis levels independent of the operators, experimental conditions, or the tissue of origin. A recent study reported significant disparities in the fibrosis scores between observers using the Metavir or Ishak system, which increased between junior and qualified, senior academic pathologists.[23] The level of experience (specialization, duration, and location of practice) seemed to have a greater influence on the variability of Metavir or Ishak scores than the characteristics of the section itself. Although the CPA measurement generally detects fibrosis, the biochemical specificity of the staining methods is poor or even unknown.[24] The methods used to detect the HYP content are also complicated. The automated evaluation system, which avoids these drawbacks and recognizes the different fibrosis progression patterns in different animal models, potentially allows SHG/TPEF microscopy to be applied to diagnosis and the predictions of disease complications.

Although the automated evaluation system is very precise and highly reproducible, it deserves further commentary. The amount of fibrosis, regardless of whether it is evaluated using fibrillar collagen, is only a part of the deleterious process that leads to cirrhosis. Architectural changes, vascular shunts, and liver cell regeneration are among the other associated features that might have a significant influence on the natural progression of liver injury. These features are also evaluated when pathologists score injured tissues; however, these lesions are not considered by the automated evaluation system. Therefore, these 11 shared parameters are best used for investigating the fibrosis progression/regression patterns, but are not ideal for assessing cirrhosis.

Using SHG/TPEF imaging, this study reveals that the automated evaluation system, which combined 11 shared

parameters that correlated with the Ishak stage and model-specific parameters that differentiated different time points, may be useful for specifically, accurately, and quantitatively monitoring liver fibrosis in different animal models. Importantly, this method may greatly contribute to evaluations of experimental treatments in rodent models for which it is difficult to score fibrosis, because of the absence of well-defined scores, such as the Ishak staging and CPA evaluation systems. Undeniably, the automated evaluation system offers a reliable method that appreciably improves liver fibrosis assessments, and we anticipate that the automated evaluation system based on SHG/TPEF will be applied to assess the efficacy of antifibrotic drugs in the near future.

Supplementary Information accompanies the paper on the Laboratory Investigation website (http://www.laboratoryinvestigation.org)

ACKNOWLEDGMENTS

We thank Dean CS Tai for his constructive comments on this study and for critically reading the manuscript. This work was supported by grants from the China National Science and Technology Major Project for Infectious Diseases Control during the 12th Five-Year Plan Period (2012ZX10002003 and 2012ZX10002005), the Major Project of National Science and Technology 'Creation of major new drugs' (2012ZX09303019), and the Peking University Medical Interdisciplinary Joint Seed Fund (M-E 201402).

DISCLOSURE/CONFLICT OF INTEREST

The authors declare no conflict of interest.

1. Lee YA, Wallace MC, Friedman SL. Pathobiology of liver fibrosis: a translational success story. Gut 2015;64:830–841.
2. Karsdal MA, Manon-Jensen T, Genovese F, *et al.* Novel insights into the function and dynamics of extracellular matrix in liver fibrosis. Am J Physiol Gastrointest Liver Physiol 2015;308:G807–G830.
3. Lee YA, Friedman SL. Reversal, maintenance or progression: what happens to the liver after a virologic cure of hepatitis C? Antiviral Res 2014;107:23–30.
4. Puche JE, Saiman Y, Friedman SL. Hepatic stellate cells and liver fibrosis. Compr Physiol 2013;3:1473–1492.
5. Trautwein C, Friedman SL, Schuppan D, *et al.* Hepatic fibrosis: concept to treatment. J Hepatol 2015;62:S15–S24.
6. Mathews S, Xu M, Wang H, *et al.* Animals models of gastrointestinal and liver diseases. Animal models of alcohol-induced liver disease: pathophysiology, translational relevance, and challenges. Am J Physiol Gastrointest Liver Physiol 2014;306:G819–G823.
7. Liu Y, Meyer C, Xu C, *et al.* Animal models of chronic liver diseases. Am J Physiol Gastrointest Liver Physiol 2013;304:G449–G468.
8. Strupler M, Hernest M, Fligny C, *et al.* Second harmonic microscopy to quantify renal interstitial fibrosis and arterial remodeling. J Biomed Opt 2008;13:054041.
9. Tai DC, Tan N, Xu S, *et al.* Fibro-C-Index: comprehensive, morphology-based quantification of liver fibrosis using second harmonic generation and two-photon microscopy. J Biomed Opt 2009;14:044013.
10. Sun W, Chang S, Tai DC, *et al.* Nonlinear optical microscopy: use of second harmonic generation and two-photon microscopy for automated quantitative liver fibrosis studies. J Biomed Opt 2008;13:064010.
11. Strupler M, Pena AM, Hernest M, *et al.* Second harmonic imaging and scoring of collagen in fibrotic tissues. Opt Express 2007;15:4054–4065.
12. Xu S, Wang Y, Tai DC, *et al.* qFibrosis: a fully-quantitative innovative method incorporating histological features to facilitate accurate fibrosis scoring in animal model and chronic hepatitis B patients. J Hepatol 2014;61:260–269.
13. Asselah T, Marcellin P, Bedossa P. Improving performance of liver biopsy in fibrosis assessment. J Hepatol 2014;61:193–195.
14. Wang TH, Chen TC, Teng X, *et al.* Automated biphasic morphological assessment of hepatitis B-related liver fibrosis using second harmonic generation microscopy. Sci Rep 2015;5:12962.
15. Sevrain D, Dubreuil M, Dolman GE, *et al.* Evaluation of area-based collagen scoring by nonlinear microscopy in chronic hepatitis C-induced liver fibrosis. Biomed Opt Express 2015;6:1209–1218.
16. Li X, Benjamin IS, Alexander B. Reproducible production of thioacetamide-induced macronodular cirrhosis in the rat with no mortality. J Hepatol 2002;36:488–493.
17. Symeonidis A, Trams EG. Morphologic and functional changes in the livers of rats after ligation or excision of the common bile duct. Am J Pathol 1957;33:13–27.
18. Ishak K, Baptista A, Bianchi L, *et al.* Histological grading and staging of chronic hepatitis. J Hepatol 1995;22:696–699.
19. Zhou XM, Cao ZD, Xiao N, *et al.* Inhibitory effects of amines from citrus reticulata on bleomycin-induced pulmonary fibrosis in rats. Int J Mol Med 2016;37:339–346.
20. Chang C, Lin CJ. LIBSVM: a library for support vector machines. ACM Trans Intell Syst Technol 2011;27:1–27.
21. Starkel P, Leclercq IA. Animal models for the study of hepatic fibrosis. Best Pract Res Clin Gastroenterol 2011;25:319–333.
22. Goodman ZD, Becker Jr RL , Pockros PJ, *et al.* Progression of fibrosis in advanced chronic hepatitis C: evaluation by morphometric image analysis. Hepatology 2007;45:886–894.
23. Rousselet MC, Michalak S, Dupré F, *et al.* Sources of variability in histological scoring of chronic viral hepatitis. Hepatology 2005;41:257–264.
24. Patel K, Bedossa P, Castera L. Diagnosis of liver fibrosis: present and future. Semin Liver Dis 2015;35:166–183.